[20] M. Gandelsonas, "Linguistic and semiotic models in architecture," *op. cit.* [1].
[21] A. Rosenfeld, "Multidimensional formal languages," *op. cit.* [1].
[22] W. R. Spillers, "Some problems of structural design," *op. cit.* [1].
[23] G. Stiny and J. Gips, "Formalization of analysis and design in the arts," *op. cit.* [1].
[24] G. Cranz, "Using Parsonean structural-functionalism for environmental design," *op. cit.* [1].
[25] J. P. Roth, "Function design," *op. cit.* [1].
[26] M. A. Harrison, "Some linguistic issues in design," *op. cit.* [1].
[27] F. Freudenstein and L. Dobrjankyj, "Some applications of graph theory to the structural analysis of mechanisms," *ASME Trans.*, vol. 93B, pp. 176–192, Feb. 1971.
[28] E. Soylemez, "Logical functional design and optimization of mechanisms and mechanical systems," Ph.D. dissertation, Columbia University, New York, 1974.
[29] L. A. Zadeh, "A linguistic approach to system analysis," *op. cit.* [1].
[30] Shen Lin, "Heuristic programming as an aid to network design," Bell Lab. Tech. Rep. (Murray Hill, N.J.), Dec. 1974.
[31] R. H. Atkin, "From cohomology in physics to ϕ-connectivity in social science," *Inter. J. Man-Machine Studies*, vol. 4, pp. 139–167, 1974.
[32] ——, "An approach to structure in architecture and urban design, 1, Introduction and mathematical theory," *Environment and Planning B*, vol. 1, pp. 51–67, 1974.
[33] J. C. Jones, *Design Methods*. New York: Wiley-Interscience, 1970.
[34] C. Alexander, *Notes on the Synthesis of Form*. Cambridge, Mass.: Harvard Univ. Press, 1964.
[35] G. T. Herman and G. Rosenberg, *Developmental Systems and Languages*. Amsterdam, The Netherlands: North-Holland, 1975.

Understanding Shape: II. Symmetry

LARRY S. DAVIS

***Abstract*—Methods of detecting approximate local symmetries of a polygon are developed, and a hierarchical representation of these symmetries is constructed. The approach is extended to a class of closed curves that have simple polygonal approximations; extension to wider classes of curves is also discussed.**

I. Introduction

The perception of shape plays a prominent role in both human and computer vision. The development of computational models for shape has closely paralleled the succession of metaphors for pattern (and, in particular, shape) recognition. Twenty years ago the metaphor was template matching, and shapes were represented by (idealized) templates. A few years later, shapes and patterns were being recognized on the basis of global feature measurements (e.g., moments, Fourier coefficients), and feature vectors served as shape representations. (The corresponding development in human perception was the extensive study of "shape psychophysics" (see Zusne [10]) during the 1960's.) More recently, there has been great interest in "syntactic" pattern recognition techniques, which analyze patterns by a "parsing" process of hierarchical decomposition. This suggests that it might be appropriate to study hierarchical shape representations.

In [1] it was suggested that the representation of the sides and angles of a simple closed curve should be hierarchical. The top levels of the hierarchy would contain a coarse description of the shape, while the lower levels would reflect the finer structure of the contour.

Other aspects of shape understanding can also be naturally described in a hierarchical fashion—in particular, symmetry. (We shall consider here only symmetry with respect to a line, i.e., lateral symmetry. Our methods could be extended to handle radial symmetry, if desired.) Symmetry can play many roles in a theory of shape understanding. If a shape is symmetric, then it can be represented economically—one need only store a description of "half" of the shape, and note the presence of the axis of symmetry. The "half" may itself possess symmetry, so that further economy is possible; this indicates the hierarchical nature of symmetry. Furthermore, if one is presented with a contour that is partially occluded (e.g., Fig. 1), the presence of symmetry in the available segments can provide powerful clues for proposing a completion to the figure. (Consideration of contours with gaps precludes using schemes based on moments (Zusne [10]) or Fourier coefficients (Zahn [9]) to detect symmetries.) In view of the difficulty in obtaining closed borders of objects from digital images using edge detection and tracking techniques (see, e.g., Davis [1]), this could be a very useful tool. The symmetry of a shape can also help in defining the orientation of the shape. Symmetry plays an important part in human perception of shape orientation (Rock [6]); a computational model for shape orientation would be useful for shape matching. By combining the orientation of a shape with notions of "top" and "bottom," an anchor can be provided for matching processes.

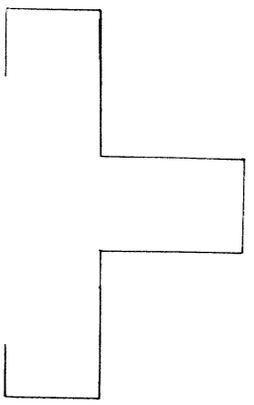

Fig. 1.

It is the contention of this correspondence that the construction of representations that capture the symmetry of a figure involves abstract symbolic processes that create hierarchical descriptions. We will first consider symmetries of simple polygons, ignoring hierarchical side/angle structure (if any). Symmetries of simple curves, and of figures that do have a hierarchical side/angle structure, will be discussed in later sections.

II. Building Hierarchical Descriptions of Symmetry for Polygons

The overall strategy for building hierarchical descriptions of the symmetries in a polygon is to first detect "microsymmetries" between pairs of sides of the polygon. Next, these microsymmetries are clustered into larger aggregates. Certain relations among these aggregates are then defined, and these relations determine the possible hierarchical descriptions of the polygon.

Suppose that we have a polygon $P = \{v_i\}_{i=0}^{n}$, where v_i are the vertices of the polygon. Let (x_{v_i}, y_{v_i}) be the coordinates of the ith vertex, and let $\mathcal{S}_i = \overrightarrow{v_i v_{i+1 \bmod n}}$ be the sides of the polygon. The first relation to determine is which pairs of sides, $(\mathcal{S}_j, \mathcal{S}_k)$, are symmetric to one another. This involves hypothesizing an axis of symmetry for the two sides, and then measuring the cost of the symmetry with respect to that axis. There are two cases to consider:

1) sides $\mathcal{S}_j$ and $\mathcal{S}_k$ meet at a vertex—i.e., either $j = k + 1 \bmod n$ or $k = j + 1 \bmod n$;
2) sides $\mathcal{S}_j$ and $\mathcal{S}_k$ do not meet.

Manuscript received May 11, 1976; revised November 1, 1976. This work was supported by the National Science Foundation under Grant MCS-72-03610-A04.

The author is with the Computer Science Center, University of Maryland, College Park, MD 20742.

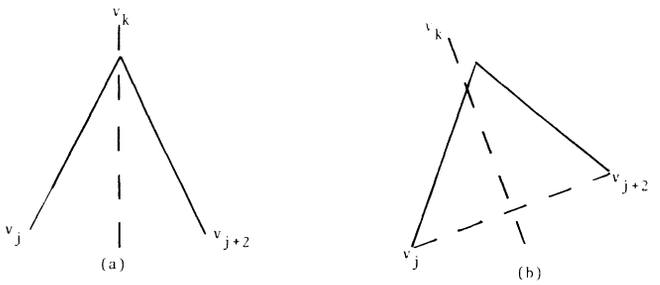

Fig. 2.

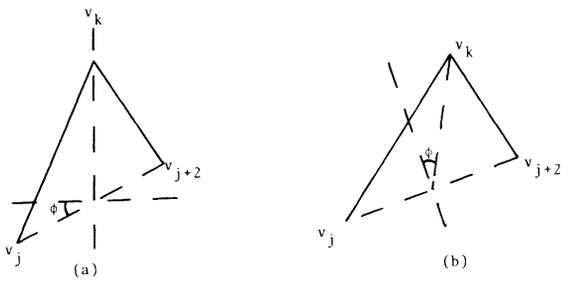

Fig. 3.

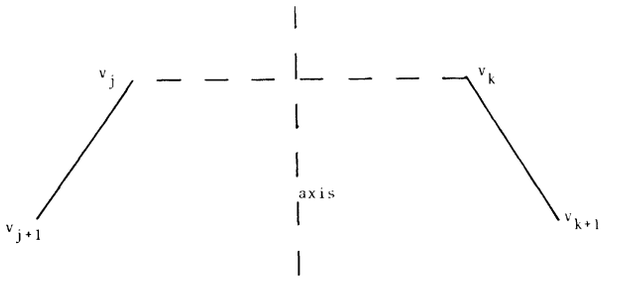

Fig. 4.

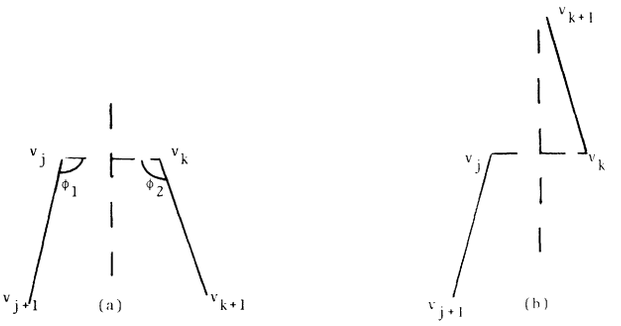

Fig. 5.

Case 1 (all numbers modulo n): Sides $\mathcal{S}_j$ and $\mathcal{S}_k$ meet at a vertex. Suppose $k = j + 1$. Then the two sides meet at vertex v_{j+1}. A likely candidate for the axis of symmetry a is either

1) the angle bisector of vertex v_{j+1}, or
2) the perpendicular bisector of the line joining vertices v_j and v_{j+2} (see Fig. 2(a), (b)).

A good measure of the cost of the symmetry $c(a)$ in this case is just the difference in the lengths of sides $\mathcal{S}_j$ and $\mathcal{S}_k$. However, it would be better for the measure to be scale invariant; the cost is related to angle ϕ in Fig. 3(a), (b). If ϕ is 0°, then the symmetry is perfect. If $\phi > 0°$, then the symmetry deviates from the ideal.

Case 2. Sides $\mathcal{S}_j$ and $\mathcal{S}_k$ do not meet. In this second case, there are four possible axes, one for each pairing of an end of $\mathcal{S}_j$ with an end of $\mathcal{S}_k$. If the pairing is (v_j,v_k) then the hypothesized axis a is the perpendicular bisector of the line joining v_j and v_k (see Fig. 4). The measure of the cost of the symmetry is (see Fig. 5(a), (b)):

a) $|\phi_1 - \phi_2|$ if v_{j+1} and v_{k+1} are in the same half plane with respect to the line v_jv_k;
b) otherwise some high number.

In practice, a threshold is set on these cost measures, and any proposed symmetry with higher cost is discarded.

The next stage of the process is to cluster the local axes of symmetry into aggregates. If each axis, a_i is represented by an equation of the form

$$\rho_i = -x \sin \theta_i + y \cos \theta_i$$

then clusters of local axes correspond to clusters of points in (ρ,θ) space [7]. The clustering algorithm designed here for grouping axes works in the following way:

Define the span of an axis, span (a_i), as the set of sides that are symmetric with respect to that axis. Define the span fraction $s(a_i)$ as the ratio of the length of span (a_i) to the perimeter of the polygon. Choose a local axis having minimal cost and maximal span as a cluster center. Call this cluster A_i. Let

$$P_i = \sum_{a_i \in A_i} \rho_i / |A_i|$$

and

$$\theta_i = \sum_{a_i \in A_i} \theta_i / |A_i|.$$

Now find a local axis a_j having minimal cost and maximal span, satisfying

a) $|\theta_i - \theta_j| < t_\theta$
b) $|\rho_i - \rho_j| < t_\rho$

where t_θ and t_ρ are dynamically defined thresholds that depend on A_i (e.g., t_ρ may be the standard deviation of the ρ_i's). If no such a_j exists, then the cluster is complete, and a new cluster can be constructed from the remaining local axes. The process continues until all local axes belong to some cluster.

Two examples of the local axes determination and clustering procedures are shown in Fig. 6. Fig. 6(a), (b) shows the polygons, with the sides and vertices labeled. Fig. 6(c), (e) are tables of the local axes detected in the polygons. (Note in Fig. 6(e) that many of the local axes do not correspond to any axis that would ordinarily be perceived by a human observer.) Fig. 6(d), (f) list the clusters constructed from the local axes.

These clusters form the basic units with which subsequent processes will work. These processes will construct hierarchical representations of the symmetries of the polygon. An example of the types of representation that will be constructed should clarify the later discussion of how the processes work. Consider Fig. 6(b), and the list of clusters for that polygon in Fig. 6(f). Fig. 7 shows one possible description of the symmetries of Fig. 6(b). The level 1 description indicates that the vertical axis comprises the highest level (level 1) of the hierarchy. It splits the figure in "half" and enables us to concentrate on finding representations of the symmetries in only half the figure. Next, level 2 contains a horizontal axis that spans all of the sides in half of the level 1 representation. Similarly, the level 3 description contains just the diagonal axis that spans all of the level 2 sides.

This example indicates that the first step in building a hierarchical symmetry representation is to chose an axis for level 1. A reasonable choice is one that "accounts for" the largest

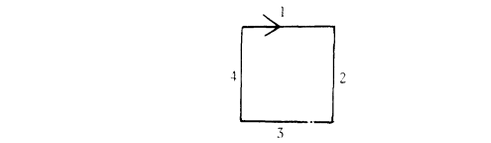

(a)

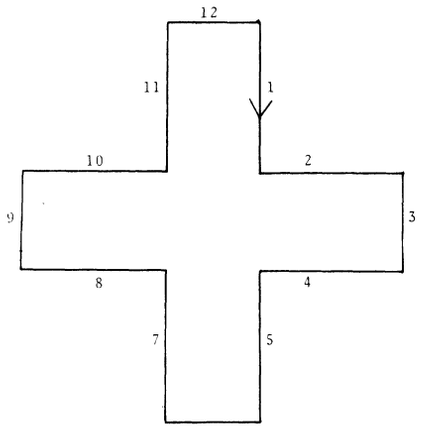

(b)

AXIS	SIDE1	ANGLE1	SIDE2	ANGLE2	THETA	RHO
1	1	1	2	2	2.3570	-113.14
2	1	2	2	1	2.3570	-113.14
3	1	1	3	2	1.5716	-80.08
4	1	2	3	1	1.5716	-80.05
5	1	1	4	2	.7862	-.09
6	1	2	4	1	.7862	-.09
7	2	1	3	2	.7862	-.09
8	2	2	3	1	.7862	-.09
9	2	1	4	2	.0008	79.92
10	2	2	4	1	.0008	79.95
11	3	1	4	2	2.3570	-113.14
12	3	2	4	1	2.3570	-113.14
13	1	1	1	2	.0008	79.92
14	2	1	2	2	1.5716	-80.05
15	3	1	3	2	.0008	79.95
16	4	1	4	2	1.5716	-80.08

(c)

NODE	THAVG	RHOAVG	AXLIST
1	235	-113	1
			11
2	157	- 80	3
			14
			16
3	78	0	5
			7
4	0	80	9
			13
			15

(d)

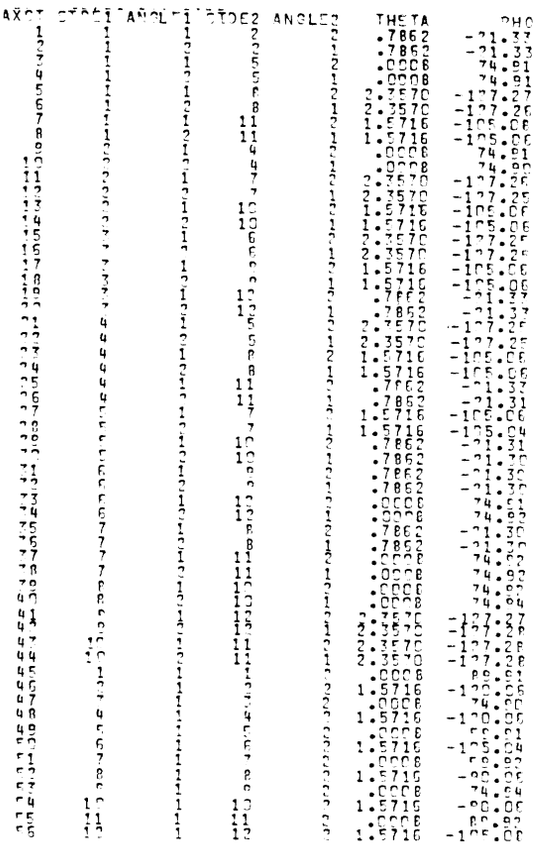

(e)

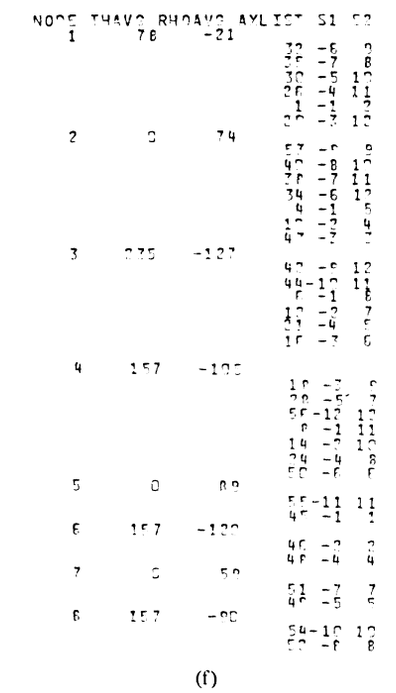

(f)

Fig. 6. (c) List of axes for (a). (d) Clusters for (a). (e) Axes for (b). (f) Clusters for (b). *Note:* For each side, angle 1 is tail of arrow and angle 2 is head (for (c)-(f)).

amount of the polygon in the best way. The particular figure of merit that was adopted here was to find the cluster A_i such that $\sum_{a_i \in A_i} s(a_i)$ is maximal, while $\sum_{a_i \in A_i} c(a_i)$ is minimal; i.e., the cluster that accounts for the greatest part of the perimeter at minimal cost. To avoid building descriptions of figures that are simply not symmetric, a threshold is placed on the $\sum_{a_i \in A_i} s(a_i)$ term. If no cluster accounts for an appreciable percentage of the polygon, then no description is generated. On the other hand, there may be several equally good clusters (as is the case for both polygons in Fig. 6). In this case, many hierarchies of symmetry

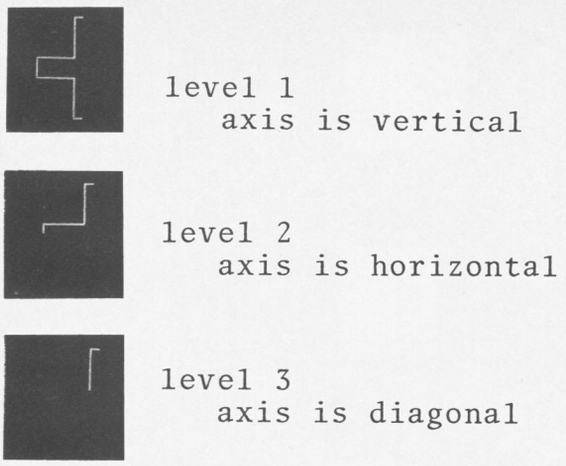

Fig. 7.

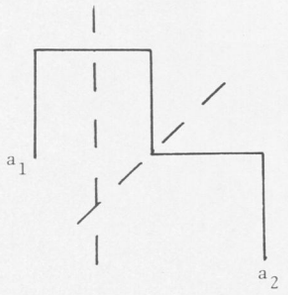

Fig. 8.

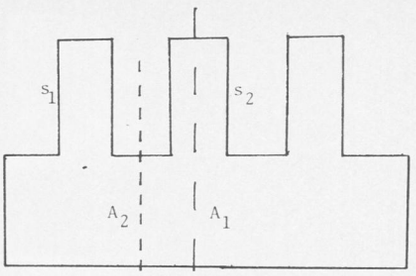

Fig. 9.

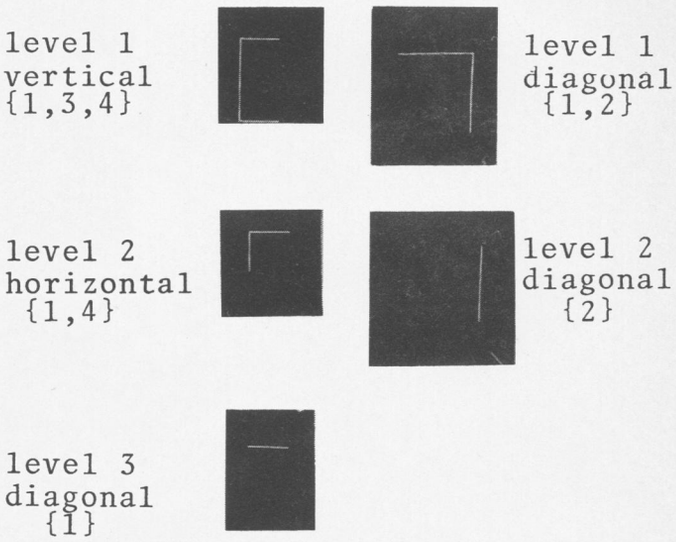

Fig. 10.

are possible. At times it may be necessary to create them all; or, there may be *a priori* biases concerning the "best" level 1 axis (e.g., the longest, the one closest to vertical). These biases will tend to affect the control of the description building mechanism, but not their underlying computations (see the recent papers by Marr [4], [5] on the role of context in low level vision).

The level 1, or major, axis splits the polygon into two sets of vertices—those in the positive half plane determined by that axis, and those in the negative half plane. The next phase of the process involves finding a set of clusters that account for the symmetries between the sides of the polygon that have at least one vertex in the positive half plane of the major axis. In order to do this we made use of two definitions:

Definition 1: Two clusters of axes A_1 and A_2 will be called *incompatible* if there exist $a_1 \in A_1$ and $a_2 \in A_2$ such that span $(a_1) \cap$ span $(a_2) \neq \varnothing$.

The notion of incompatibility tries to capture the fact that there are pairs of axes of a figure that cannot be attended to simultaneously. For example, in Fig. 8, the axes a_1 and a_2 are incompatible. It should be pointed out that incompatibility is a relation that is only meaningful when comparing two axes at the same level in the hierarchy—i.e., if two clusters are incompatible this means that they cannot both occur at the same level of the hierarchy. However, it is quite possible for them to occur at different levels. A relation that extends across levels in the hierarchy is:

Definition 2: A_2 is *inconsistent* with respect to A_1 if there exists an $a_2 \in A_2$ such that elements of span (a_2) occur entirely in both the positive and negative half planes determined by A_1. For example, in Fig. 9, A_2 is inconsistent with respect to A_1 because sides s_1 and s_2 are contained one in the positive, and the other in the negative, half plane defined by A_1.

Given these two definitions, we are now in a position to describe the construction of the lower levels of the hierarchy. Call a node N in the hierarchy a tip node if the operation described below has not been applied to it. Initially, the root of the hierarchy, which corresponds to the major axis, is the only tip node. Each node has an axis A_N associated with it. Let S_N be the set of sides of the polygon associated with the tip node. At the root initially, S_N is the set of sides of the polygon that

a) are symmetric with respect to the major axis,
b) have at least one vertex in the positive half plane defined by the major axis.

The expansion operation is as follows.

1) Choose a tip node N from the hierarchy—if there are none, then the hierarchy is complete.

2) Find all clusters A_i such that a) A_i is not already in the hierarchy, and b) A_i is not inconsistent with respect to A_N.

Let PD be the set of these A_i; PD represents the set of possible descendants of node N in the hierarchy. Let D_N be the set of descendants of node N. Initialize $D_N = \varnothing$.

3) Choose from PD the axis A_j such that $s(\text{span}\,(A_j \cap S_N)) > 0$ is maximal, and A_j is not incompatible with any element of D_N. If no such A_j exists, then all of the descendants of node N have been generated, and we go to step (1).

4) Set $S_N = S_N - (\text{span}\,(A_j) \cap S_N)$. Set $PD = PD - A_j$, and $D_N = D_N \cup A_j$. Insert node N' into the hierarchy with $A_{N'} = A_j$, and $S_{N'} = \{\mathcal{S}_i \mid \mathcal{S}_i \in \text{span}\,(A_j) \cap S_N$ and $\mathcal{S}_i$ is in the positive half plane determined by axis $A_j\}$. Go back to step (4).

Given different major axes, different hierarchies will be generated. Fig. 10 shows two such hierarchies for the square in Fig. 6(a). At each node in the hierarchy we display S_N and

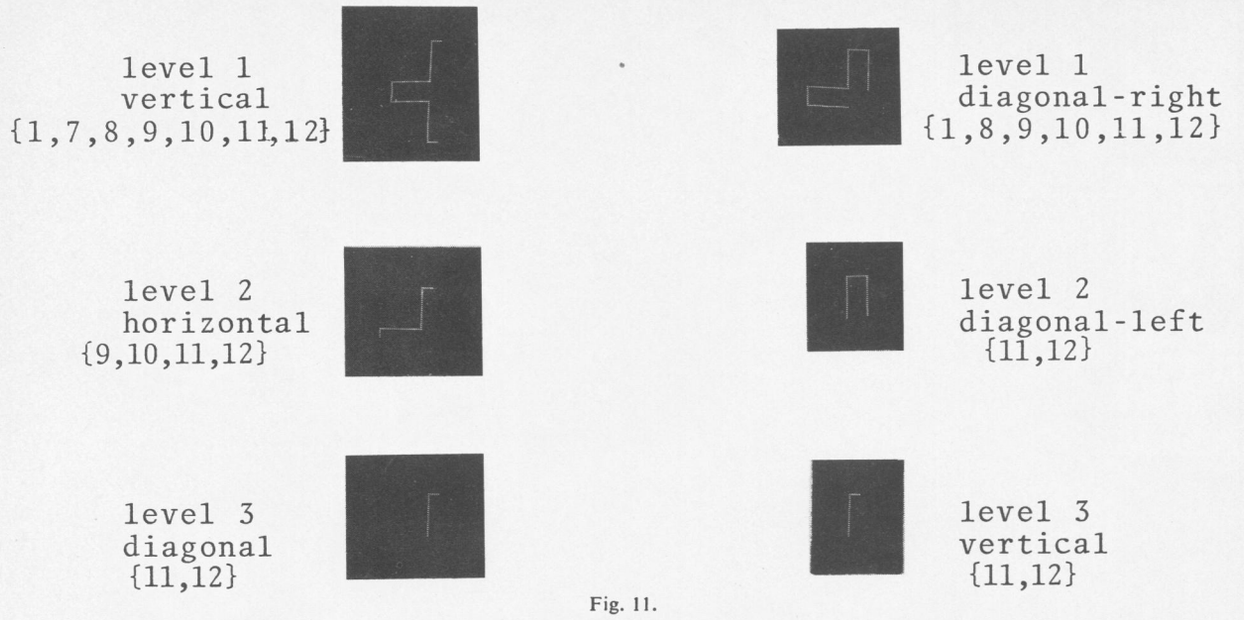

Fig. 11.

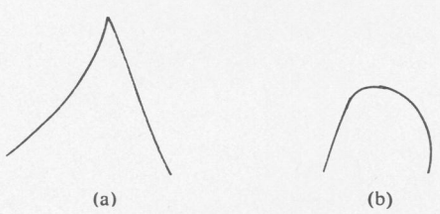

Fig. 12. (a) Sharp angle. (b) Blunt angle.

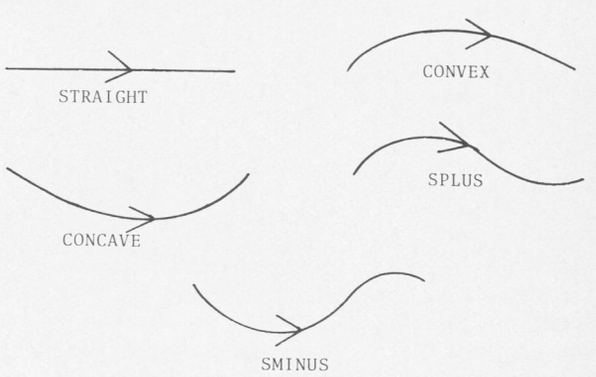

Fig. 13.

list the axis associated with that node. Fig. 11 contains two hierarchies for the cross in Fig. 6(b).

III. Extension to Smoothly Curved Sides

This section will consider how the approach described in Section II is modified to deal with sides that may curve gently. A smooth curve segment is taken to be one with no significant curvature maxima. Significance is a function of both the resolution and magnitude of the curvature maxima that do exist along a curve segment. In the context of hierarchical descriptions, a smooth side is a side with no substructure. Thus the process that constructs the hierarchical description implicitly defines the significance of curvature maxima.

In order to augment the symmetry understanding mechanisms to deal with smooth curves, a notion of shape similarity is incorporated into the microsymmetry detection procedures. It is important to emphasize that we are interested in coarse measures of similarity; therefore, curves that are exactly similar according to the criteria we will define will not necessarily be identical. The problem of matching two curves will be discussed elsewhere. This entails modifying the microsymmetry cost function c to reflect the degree of similarity between two curves. A second, more subtle, difference between contours with smooth sides and these with only straight sides is that angles may no longer be corners; an angle may be sharp or blunt, depending on the curves that meet at the angle (see Fig. 12). Here again, the microsymmetry cost function is where this new information enters the system. This means that neither the cluster building nor description building procedures have to be changed.

The remainder of this section is divided into three parts:

A) A discussion of similarity measures between smooth curves.

B) A discussion of functions that compute the "sharpness" of an angle.

C) Analysis results for some smoothly curved contours.

A. Similarity Measures Between Smooth Curves

Our similarity measure is based on assigning fuzzy memberships in a class of sets to a curve. The sets correspond to the allowable description types for the class of contours being considered—e.g., straight, convex, concave. The names of these sets constitute a vocabulary for describing smooth sides. We will consider only the following five descriptions—STRAIGHT, CONVEX, CONCAVE, SPLUS, SMINUS (see Fig. 13).

Let the sequence of coordinate pairs of a side s_i be

$$v_i = (x_{i_0},y_{i_0}),(x_{i_1},y_{i_1}),\cdots,(x_{i_n},y_{i_n}) = v_{i+1}.$$

Let $b_{s_i} = (\theta_{s_i},\rho_{s_i})$ be the parametric description of the straight side in the hierarchy of sides corresponding to s_i. For example, b_{s_i} might be $\overrightarrow{v_i v_{i+1}}$. A particularly bad choice is the least squares line defined by the points $(x_{i_0},x_{i_1}),\cdots,(x_{i_n},y_{i_n})$, since it must pass through one of the points in the sequence. Let $d(x,y,b_s) = \rho_s - x \sin\theta_s + y \cos\theta_s$ be the distance of the point (x,y) from the line b_s.

The first step in determining the membership values for s_i is to construct the set

$$\mathcal{D}_{s_i} = \{d(x_{i_j},y_{i_j},b_{s_i}): 1 \le j \le n-1\}$$

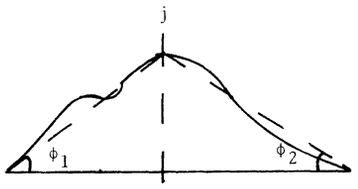

Fig. 14.

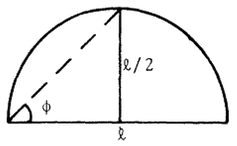

Fig. 15.

which is the set of distances of all points of s_i from b_{s_i}. Define

$$\mathcal{D}^+_{s_i,r} = \{j: d(x_{i_j},y_{i_j},b_{s_i}) > 0 \wedge d(x_{i_k},y_{i_k},b_{s_i}) < d(x_{i_j},y_{i_j},b_{s_i}), \quad |j-k| \le r\}$$

$$\mathcal{D}^-_{s_i,r} = \{j: d(x_{i_j},y_{i_j},b_{s_i}) < 0 \wedge d(x_{i_k},y_{i_k},b_{s_i}) > d(x_{i_j},y_{i_j},b_{s_i}), \quad |j-k| \le r\}.$$

$\mathcal{D}^+_{s_i,r}$ is the set of points that are local maxima of distance from b_{s_i} over a range (smoothing factor r), and $\mathcal{D}^-_{s_i,r}$ similarly is the set of local minima. We should choose r large enough so that the local distance maxima corresponding to curvature maxima of fine resolution will not be detected. $\mathcal{D}^+_{s_i,r}$ can be computed by a parallel-like algorithm (see Davis [1]).

We sort $\mathcal{D}^+_{s_i,r}$ by d so that we can refer to $\mathcal{D}^+_{s_i,r}(1)$, the element of the set with greatest d value, etc. Similarly, we sort $\mathcal{D}^-_{s_i,r}$ so that $\mathcal{D}^-_{s_i,r}(1)$ is the element of the set with minimal d value. We use the ordered sets $\mathcal{D}^+$ and $\mathcal{D}^-$ to construct the fuzzy membership values for side s_i. Denote $\mathcal{D}^+_{s_i,r}(1)$ by i^+ and $\mathcal{D}^-_{s_i,r}(1)$ by i^-. If $\mathcal{D}^+$ is empty, let $i^+ = -1$, and similarly for $\mathcal{D}^-$. We can now present the fuzzy membership functions for the various sets.

1) STRAIGHT: We take the ideal straight side to be one whose $\mathcal{D}^+$ and $\mathcal{D}^-$ are empty. The straightness of a side is related to the angular stickout of the elements of $\mathcal{D}^+$ and $\mathcal{D}^-$ from the line b_{s_i}. The angular stickout of point (x_{i_j},y_{i_j}) from b_{s_i} is (see Fig. 14)

$$ASO(j) = \frac{\sin^{-1}(|d(x_{i_j},y_{i_j},b_{s_i})|}{\max[\sqrt{(x_{i_0}-x_{i_j})^2+(y_{i_0}-y_{i_j})^2}, \sqrt{(x_{i_n}-x_{i_j})^2+(y_{i_n}-y_{i_j})^2}]}, \quad \text{if } 1 \le j \le n$$
$$= 0, \quad \text{otherwise.}$$

If $i^+ = -1$, then $ASO(i^+) = 0$. To measure STRAIGHT (s_i), then, we compute

$$\max(0,(\max(ASO(i^+),ASO(i^-)) - t_{ST}) \cdot (1/t_{ST}))$$

That is, the straightness of side s_i is related to the maximum angular stickout of any point of side s_i from b_{s_i}. If this angular stickout is greater than some threshold t_{ST}, we set the membership of s_i in the set STRAIGHT to 0. t_{ST} will correspond to the angular stickout of an ideal convex side. Thus we are saying that a side whose membership in CONVEX is 1.0 has membership 0 in STRAIGHT.

2) CONVEX: Our model for a convex side is a semicircle. For side s_i of length $l = |\overrightarrow{v_i v_{i+1}}|$, a semicircle with s_i as diameter will have maximum angular stickout from b_{s_i} of $\pi/4$ (see Fig. 15). So, we define CONVEX $(s_i) = \min(ASO(i^+) - ASO(i^-),0) \cdot 4/\pi$. If $ASO(i^-) > ASO(i^+)$, then the side is more concave than convex.

3) CONCAVE $(s_i) = \min(ASO(i^-) - ASO(i^+),0) \cdot 4/\pi$.

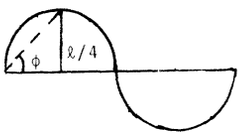

Fig. 16.

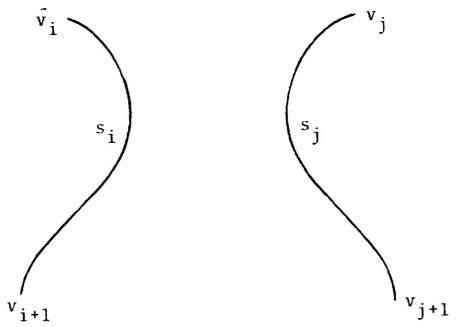

Fig. 17.

4) SPLUS: This case represents smooth sides that have a convex segment followed by a concave segment. Clearly SPLUS blends into STRAIGHT, CONVEX, and CONCAVE as the ASO values go to 0, or the lengths of the convex or concave segments go to 0. Our model for an SPLUS side is a convex semicircular arc joined with its reflection, a concave semicircular arc (see Fig. 16), and we take

$$\text{SPLUS}(i,s_i) = \text{if } i^+ < 0 \vee i^- < 0, \text{ then } 0,$$
$$\text{else if } i^- < i^+, \text{ then } 0,$$
$$\text{else } \min(ASO(i^+), ASO(i^-)) \cdot 1/t_{SP},$$

where $t_{SP} = \pi/8$ (see Fig. 16).

5) SMINUS is defined analogously to SPLUS.

Using these functions, a side is assigned a membership in each set. As a measure of dissimilarity between two sides we have chosen the maximum absolute difference between corresponding membership values. The cost function for microsymmetries is changed in the following way. Any pair of sides not symmetric according to the old criterion is rejected, but now any pair of sides whose dissimilarity measure >0.5 is also rejected. The value 0.5 was chosen because it indicates a reasonable certainty that one side is contained in one set (e.g., CONVEX), while the other side is not.[1] The new value for the cost is the old value plus a scale factor times the dissimilarity:

$$c'(a) = c(a) + k \cdot \text{dissimilarity of } (s_i,s_j).$$

B. "Cornerity" Measurement

In [3], Freeman and Davis proposed a "cornerity" measure that was based on the curvature at an angle and the straightness of the sides of that angle. This section presents an alternative method based on the local curvature measurements that underlie the angle detection procedures described in Davis [1].

Briefly, this curvature measure is defined as follows: Let $\{(x_i,y_i)\}_{i=0}^n$ be a sequence of points that describe a simple curve. Let $\vec{p}_{i,j}$ be the vector from (x_i,y_i) to (x_j,y_j). Then $c_{i,r}$, the curvature at point i and resolution r, is defined to be $\cos^{-1}(\vec{p}_{i,i-r} \cdot \vec{p}_{i,i+r})$. This is the size of the smaller included angle determined by the two vectors.

[1] Note that when computing the dissimilarity between s_I and s_J for determining the degree of microsymmetry between the sides, if we are using vertex pairs v_I and v_{J+1} (or v_{I+1} and v_J), then we compare SPLUS (s_I) with SMINUS (s_J) and SMINUS (s_I) with SPLUS (s_J)—see Fig. 17.

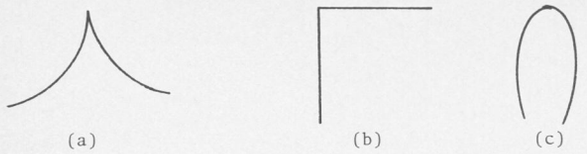

Fig. 18.

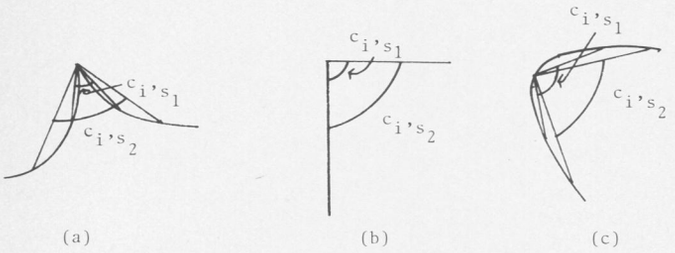

Fig. 19.

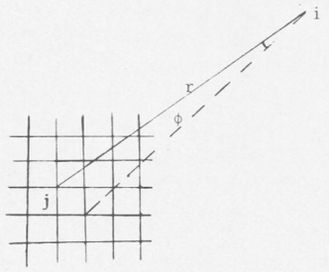

Fig. 20.

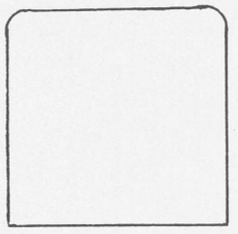

Fig. 21.

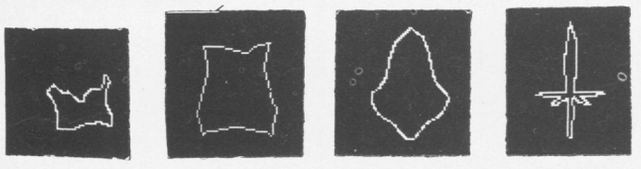

Fig. 22. Test curves.

Now, suppose that the angles in Fig. 18 are to be distinguished on the basis of their sharpness. The angle in Fig. 18(a) can be described as cusp-like, that in Fig. 18(b) as corner-like, and that in Fig. 18(c) as rounded.

The method is based on the rate of change of $c_{i,r}$ with respect to r—i.e., $dc_{i,r}/dr$. Fig. 19(a)–(c) shows that we would expect $dc_{i,r}/dr$ to be positive for a cusp-like angle, zero for a corner-like angle, and negative for a rounded angle.

In order to estimate $dc_{i,r}/dr$, we fit a least squares line to a set of $c_{i,r}$'s and regard the slope as $dc_{i,r}/dr$. Since different resolutions are attributed to different angles, the set of $c_{i,r}$'s used to calculate $dc_{i,r}/dr$ for a particular angle should be determined by the resolution of that angle. The largest size used

TABLE I
FOURIER COEFFICIENTS FOR FIG. 22(c)–(d)

(a)

n	α_n	γ_n
0	20	0
1	20	0
2	20	0
3	20	0
4	20	0

$$r(\theta) = \sum_{n=0}^{4} \alpha_n \exp[\cos(\theta+\gamma_n)]$$

(b)

n	α_n	γ_n
0	4.	0
1	4.5	0
2	5.0	0
3	5.5	0
4	6.0	0

$$r(\theta) = \sum_{n=0}^{4} \exp[\alpha_n \cos(\theta+\gamma_n)]$$

TABLE II
FUZZY MEMBERSHIP VECTORS FOR THE SIDES OF FIG. 23(a)–(d)

(a)

SIDE	DEGREES OF MEMBERSHIP (STRAIGHT, CONVEX, CONCAVE, SPLUS, MINUS)
1	(.87,0,.12,0,0)
2	(.74,.25,0,0,0)
3	(.71,0,.28,0,0)
4	(.85,0,.08,0,.11)
5	(.82,0,.17,0,.11)

(b)

1	(.74,.25,0,0)
2	(.88,0,.02,.17,0)
3	(.79,.20,0,0,0)
4	(.88,0,0,0,.22)

(c)

1	(.88,.03,0,.16,0)
2	(.84,.15,0,0,0)
3	(.85,.14,0,0,0)
4	(.86,.08,0,0,.10)

(d)

1	(.92,.07,0,0,0)
2	(1.00,0,0,0,0)
3	(.70,.24,0,0,.10)
4	(.88,.11,0,0,0)
5	(1.00,0,0,0,0)
6	(.40,.54,0,.09,0)
7	(.89,.10,0,0,0)
8	(.86,.13,0,0,0)

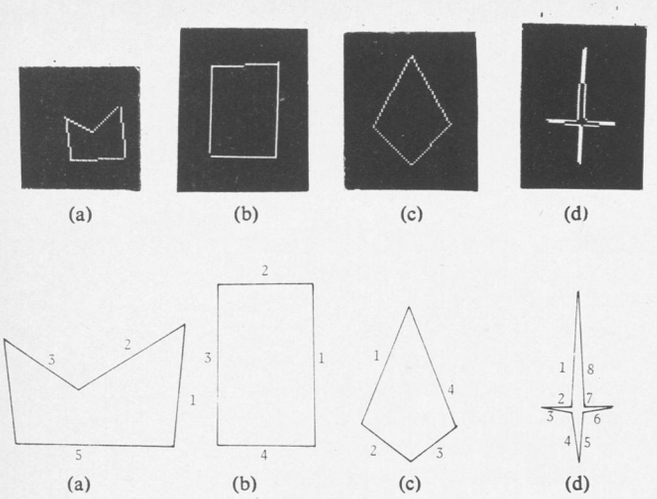

Fig. 23. Top-level approximations.

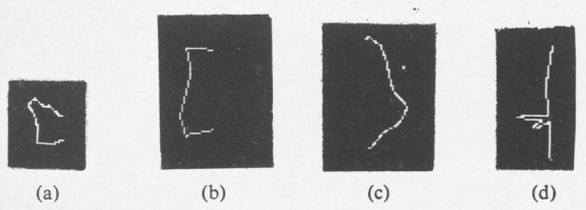

Fig. 24. "Halved" figures using best axis.

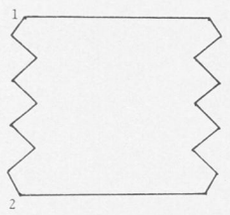

Fig. 25.

should reflect the localness of the perception of sharpness, and so will probably not usually be comparable to the resolution of the angle. The smallest size, on the other hand, should be large enough so that curve digitization error cannot appreciably influence the computations (if l is the length of $\vec{p}_{ij}$, then the angular uncertainty in $\vec{p}_{ij}$ is proportional to arctan $1/l$—see Fig. 20). Alternatively, one can weight the curvature values according to the expected error due to digitization. However, we will assume that our curves are well digitized (Freeman [2]), so that digitization effects can be ignored.

It is not obvious how to compare the importance of similar angle descriptions and side descriptions in evaluating the quality of an axis of symmetry, and so the cornerity measure has not yet been integrated into the microsymmetry cost function. Fig. 21, though, seems to indicate that the description of angles does play a role in human perception of symmetry; intuitively, its role is less important than that of side descriptions.

C. Experimental Results

Fig. 22(a)–(d) shows four smooth curves. Fig. 22(a) is a jigsaw puzzle piece taken from Freeman [2]; Fig. 22(b) is a hand-drawn square-like object; while Fig. 22(c), (d) were generated using Fourier methods due to Shepard [8] and described in Davis [1]. Table I lists the coefficients used to generate Fig. 22(c), (d).

TABLE III
CORNERITY MEASURES FOR THE ANGLES IN FIG. 23(a)–(d)

	angle	cornerity (r=8)
(a)	1	.05
	2	.16
	3	.13
	4	.28
	5	-.05
(b)	1	-.02
	2	0.
	3	.03
	4	-.01
(c)	1	-.01
	2	0.
	3	.10
	4	.01
(d)	1	0.
	2	.02
	3	0.
	4	.01
	5	.04
	6	.02
	7	0.
	8	.02

The top level of the angle/side hierarchy for each of the contours is shown in Fig. 23(a)–(d). Table II(a)–(d) lists the fuzzy membership values of each of the sides of the hierarchies in Fig. 23(a)–(d). Table III(a)–(d) displays the cornerity measures for the angles in the hierarchies, and Fig. 24(a)–(d) shows the best symmetry descriptions of each of the contours. Note that especially for Fig. 22(b), if the descriptions of the sides were not taken into account, then the vertical axis would not have been preferred over, say, the horizontal.

V. Symmetry Understanding for Hierarchical Descriptions of Shape

Suppose that instead of restricting the sides of a contour to be smooth, we allow them to have substructure in the form of subsides. (Methods of obtaining hierarchical representations of contours in terms of sides and subsides were discussed in an earlier paper [1].) For example, in Fig. 25, it does not seem sufficient to describe the side between angles 1 and 2 as simply being straight; some notice should be taken of the many small sharp angles and short sides that underlie the gross straight nature of the side. The presence of this substructure should also be taken into account when describing the symmetries of Fig. 25.

The discussion that follows will be mostly speculative; instead of presenting extensions or modifications to the algorithms of Sections II and III, we will examine certain issues that would be central to any such modifications. Some of these issues should be relevant to a computer model of human shape understanding. The first question to be dealt with is: Are the smooth sides discussed in Section III a subset of the set of

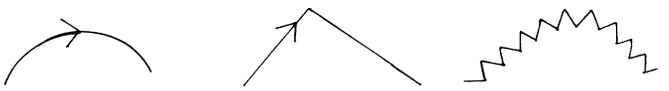

Fig. 26.

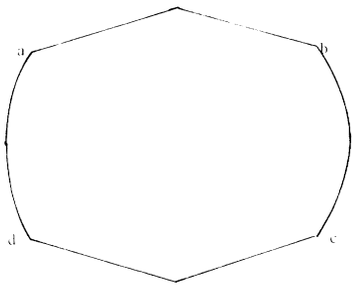

Fig. 27.


Fig. 28.


Fig. 29.

sides that have substructure, or are the sets disjoint? On the one hand, we have regarded a side as being smooth just in case it is assigned no substructure. Yet, on the other hand, a piecewise-linear approximation to a smooth side may be represented as a side with substructure, and this can happen in many ways.

For example, Fig. 26(b), (c) shows piecewise-linear approximations to the smooth curve in Fig. 26(a). If we regarded all three curve segments in Fig. 26 as smooth, and generated the sets $\mathscr{D}^+$ and $\mathscr{D}^-$, then the description generated based on these sets would probably be the same for all three segments: primarily convex curves. The substructural components of Fig. 26(b), (c) correspond to yet another level of description. Fig. 26(b) is a convex side with one obtuse angle located at the point of maximal displacement from the baseline, while Fig. 26(c) is a convex side that is jagged. This suggests that in detecting symmetries between two sides, we might compare the descriptions based on the assumption that the sides are smooth, and then refine this comparison using substructure information. So, for example, in Fig. 27, all four sides would be characterized as convex, but sides *ab* and *cd* would have have a common substructural description—namely, the obtuse angle.

Fig. 26(b), (c) also illustrates an important aspect of the representation of substructure. Fig. 26(b) has as substructure one obtuse angle, while we described the substructure of Fig. 26(c) as "jagged." The distinction between substructural description that are statistical (Fig. 26(c)) and enumerative (Fig. 26(b)) is a fuzzy one. In the former case, we are abstracting a common feature of many substructural components, and assigning that quality to the side as a whole; while in the latter case, no such global description of the side is possible. The situation can become more complex, as in Fig. 28, where there is a combination of statistical and enumerative features—i.e., we can describe the curve segment as a straight jagged segment, followed by a smooth, straight segment, followed by a straight wavy segment.

Even more perplexing is the need to notice repetitive features. Figs. 27 and 28 can probably be adequately dealt with on the basis of a simple taxonomy of angles as sharp or rounded. But in curve segments such as in Fig. 29, it is important to be able to isolate the elements ⌒ and ⌒; otherwise, we cannot obtain a satisfactory description of the curve, i.e., a description that is in accordance with our own perception.

VI. Discussion

Symmetry certainly plays a prominent role in human perception of shape. In computer understanding of shape, symmetry can serve as a basis for compact representation schemes, as well as providing clues for the completion of shapes with gaps. A subsequent report will deal with the latter problem.

The previous sections of this report have presented algorithms that can understand symmetry for polygon-like shapes, and have described modifications to these algorithms that allow the analysis of shapes with smooth sides. Several examples were presented to illustrate the capabilities of the algorithms. Finally, some of the difficulties that would be encountered in attempting to extend the symmetry analysis to shapes with a hierarchy of side and angle representations were discussed.

Acknowledgment

The help of Ms. Shelly Rowe in preparing this text is gratefully acknowledged.

References

[1] L. Davis, "Understanding shape: Angles and sides," to be published in *IEEE Trans. Comput.*
[2] H. Freeman and L. Gardner, "Apictorial jigsaw puzzles: The computer solution of a problem in pattern recognition," *IEEE Trans. Electron. Comput.*, vol. EC-13, pp. 118–127.
[3] H. Freeman and L. Davis, "A corner finding algorithm for chain-coded curves," Univ. of Maryland Tech. Rep. TR-399, Aug. 1975.
[4] D. Marr, "On the purpose of low level vision," MIT A.I. Memo 324, Dec. 1974.
[5] ——, "Analyzing natural images, a computational theory of texture vision," MIT A.I. Memo 334, June 1975.
[6] I. Rock, *Orientation and Form.* New York: Academic Press, 1973.
[7] R. Duda and P. Hart, "Use of the Hough transform to detect lines and curves in pictures," *C.ACM*, vol. 15, pp. 11–15.
[8] R. Shepard and G. Cermak, "Perceptual-cognitive explorations of a toroidal set of free form stimuli," *Cog. Psych.*, vol. 4, pp. 351–377.
[9] C. Zahn and R. Roskies, "Fourier descriptors for plane closed curves," *IEEE Trans. Comput.*, vol. C-21, pp. 269–280.
[10] L. Zusne, *Visual Perception of Form.* New York: Academic Press, 1970.

Signature Verification Experiment Based on Nonlinear Time Alignment: A Feasibility Study

MAKOTO YASUHARA, MEMBER, IEEE, AND MASATOMO OKA

***Abstract*—Automatic signature verification experiments are described, in which we select one of the most promising techniques described in the literature of automatic speech recognition of multisyllabic utterances: nonlinear time alignment by dynamic programming, and apply it to our problem to check its feasibility. Our experiments show that it is very useful under certain conditions.**

Introduction

This correspondence discusses one of the techniques applied to the automatic verification of real-time signatures.

Manuscript received July 15, 1976; revised October 25, 1976.
M. Yasuhara is with the Research Laboratory of Communication Sciences, University of Electro-Communications, Tokyo 182, Japan.
M. Oka is with Nippon Electric Co., Tokyo, Japan.